
Article:
Brookman, M. W., Austin, M. E., Petty, C. C. et al. (8 more authors) (2021) Resolving ECRH deposition broadening due to edge turbulence in DIII-D. Physics of Plasmas. 042507. ISSN 1089-7674

https://doi.org/10.1063/1.5140992

Resolving ECRH deposition broadening due to edge turbulence in DIII-D

Cite as: Phys. Plasmas **28**, 042507 (2021); https://doi.org/10.1063/1.5140992
Submitted: 05 December 2019 . Accepted: 24 March 2021 . Published Online: 21 April 2021

M. W. Brookman, M. E. Austin, C. C. Petty, R. J. La Haye, K. Barada, T. L. Rhodes, Z. Yan, A. Köhn, M. B. Thomas, J. Leddy, and R. G. L. Vann

Physics of Plasmas ARTICLE scitation.org/journal/php

Resolving ECRH deposition broadening due to edge turbulence in DIII-D

Cite as: Phys. Plasmas **28**, 042507 (2021); doi: 10.1063/1.5140992
Submitted: 5 December 2019 · Accepted: 24 March 2021 ·
Published Online: 21 April 2021

M. W. Brookman,[1,a)] M. E. Austin,[1] C. C. Petty,[2] R. J. La Haye,[2] K. Barada,[3] T. L. Rhodes,[3] Z. Yan,[4] A. Köhn,[5] M. B. Thomas,[6] J. Leddy,[6] and R. G. L. Vann[6]

AFFILIATIONS

[1]Institute for Fusion Studies, Department of Physics, University of Texas at Austin, 2515 Speedway, Austin Texas, 78712, USA
[2]General Atomics, 3550 General Atomics Ct., San Diego, California 92121, USA
[3]University of California, Los Angeles, Los Angeles, California 90005, USA
[4]University of Wisconsin-Madison, Madison, Wisconsin 53706, USA
[5]Institut für Plasmaforschung, Universität Stuttgart, 70569 Stuttgart, Germany
[6]York Plasma Institute, Department of Physics, University of York, Heslington, York YO10 5DD, United Kingdom

Note: This paper is part of the Special Collection: Papers from the 61st Annual Meeting of the APS Division of Plasma Physics.
Note: Paper TI2 6, Bull. Am. Phys. Soc. **64** (2019).
[a)]Invited speaker. **Present address:** General Atomics, 3550 General Atomics Ct., San Diego, California 92121, USA. **Author to whom correspondence should be addressed:** brookmanmw@fusion.gat.com

ABSTRACT

Microwave heat pulse propagation experiments have demonstrated a correlation between millimeter-scale turbulence and deposition profile broadening of electron cyclotron (EC) waves on the DIII-D tokamak. In a set of discharges in DIII-D, a variation in edge density fluctuations on the mm-scale is associated with 40%–150% broader deposition profiles, expressed in terms of normalized minor radius, as compared with equilibrium ray tracing. The 1D power profile is determined from transport analysis of the electron temperature response to EC power modulation using perturbative analysis with a square wave power modulation at 20–70 Hz, producing a series of Fourier harmonics that are fit collectively to resolve transport. Fitting an integrated heat flux expressed in the Fourier basis of the modulation to diffusive, convective, and coupled transport terms in a linear model can resolve the broadened EC deposition width from the power perturbation to resolve a broadening in each case. The best fit degree of beam broadening observed scales approximately linearly with the Doppler backscattering measured fluctuation level in the steep gradient region. Quantifying the effect of edge fluctuation broadening on EC current drive power needs of future devices will require 3D full-wave codes that can be validated on the current generation of machines. These DIII-D experiments provide a quantitative measure of fluctuation effects and a dataset to benchmark full-wave simulations that can model and eventually predict nonlinear effects neglected by 1D equilibrium beam and ray tracing.

I. INTRODUCTION

Electron cyclotron current drive (ECCD) is used to drive current in tokamak plasma and is the key means of stabilizing tearing modes, magnetohydrodyanmic structures that limit plasma confinement and drive disruptions.[1] An increased width of the microwave current drive profile, projected to be similar to the width of the island chain in some cases, can cause the loss of significant amounts of power when the deposition falls outside of the island O-point. The width of the deposition profile is thus highly significant to its efficiency in tearing mode suppression. Prompt response to applied power, characterized by a rapid change in transport over the perturbation cycle,[2] obscures the base deposition width. Past efforts have found agreement in deposition radius of the injected microwave beam between experiment[3] and ray-tracing code TORAY-GA,[4] but resolving the radial extent of the deposition (the deposition width), requires a self-consistent treatment of the prompt transport changes generated by power modulation.[5,6] This work presents an effort to resolve the microwave deposition profile width in a set of experiments through a self-consistency of the RF

heating, measured temperature, and transport modeling during a modulated RF pulse.

Simulations[7,8] and experimental efforts[9,11,14] have found that density fluctuations of a similar scale to the microwave vacuum wavelength produce a scattering of the well-columnated microwave beam. Propegation through the plasma edge, where mm-scale fluctuations are strongest due to the steep gradient, results in multiple interactions, increasing divergence, and wider deposition at the same power.[8] Magnetic fluctuations can theoretically also cause microwave scattering, but the predicted effect is much weaker and thus is not considered in this study.[15] For EC waves, parametric studies[8] with full-wave simulations suggest mm-scale structures with a correlation length of approximately half the RF vacuum wavelength, $\lambda_{vac} = 2.7$ mm for the 110 GHz power used on DIII-D. This study quantifies the deposition width of EC heating across a range of edge conditions over which the Doppler Backscattering measured millimeter-scale fluctuations vary by a factor of 4, sufficient to produce a first experimental scaling of beam broadening with fluctuation level.

Transport fitting can resolve deposition broadening from modulated transport coefficients by evaluating a set of trial deposition functions for consistency with a three-term linear electron heat flux model. A scaling in scattering-relevant fluctuations is achieved through analysis of multiple confinement modes with matched aiming, where the beam waist is aligned across flux surfaces at deposition, emphasizing scattering effects in the 1D profile. This study finds a substantial degree of deposition broadening, from 1.4–2.8x wider than equilibrium ray tracing and form a dataset that can be used to benchmark simulations. With modulation techniques that have already been explored on ASDEX[16] and DIII-D[17] and benchmarked by simulation,[18] this cost can be limited, with the substantial degree of broadening observed in this study suggesting such techniques will provide significant power savings.

Section II discusses a series of experiments with modulated microwave power performed with different edge conditions to study the impact of fluctuations. Section III introduces a method of fitting heat transport to resolve deposition broadening in experimental data. Section IV discusses the results of the confinement mode study and validation of this method against past transport studies. An order of magnitude variation of the scattering fluctuations allows for a scaling of deposition broadening.

II. CONNECTING MICROWAVE BROADENING TO FLUCTUATIONS

A. Defining and assessing beam broadening

The behavior of microwaves used for electron cyclotron heating (ECH) in a tokamak plasma equilibrium is frequently simuluated with quasi-optical propagation. Ray tracing is used to establish the equilibrium propagation and deposition absent scattering effects. The TORAY-GA ray-tracing code accounts for the effects of geometry and 1D temperature and density profiles, but it does not treat density fluctuations.[4]

For these discharges, geometry is selected to maximize the effects of beam waist on deposition width, with the beam waist aligned across flux surfaces by setting $B_t \approx 2.0T$. This places the X2 electron cyclotron resonance near the magnetic axis. As the beam trajectory is nearly tangent to flux surfaces near the resonant location, a wider beam will produce a correspondingly wider deposition width across flux surfaces as illustrated in Fig. 1.

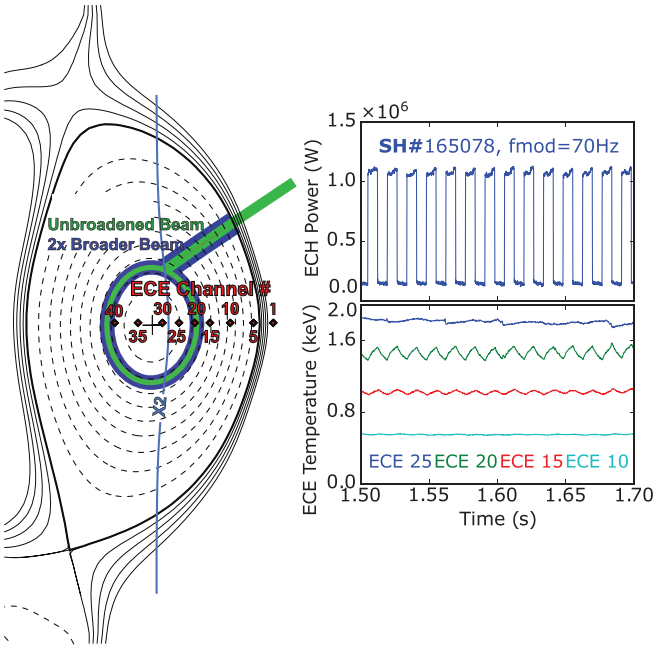

FIG. 1. Modulation in the applied gyrotron (top right) produces an electron temperature response. An equilibrium reconstruction of inner wall limited L-mode 165 078 (left), one discharge and beam aiming used in this study. An illustration of the effects of beam broadening driving broader deposition is shown for an equilibrium deposition in green with a broadened beam in blue. The location of the electron channels which measure the microwave-driven temperature perturbation are shown in red, and their response (below right) will be used to assess the deposition profile.

In the subsequent sections, a transport fitting is used to differentiate beam broadening from the transport response to ECH power modulation. To do this, a series of broadened profiles are generated and evaluated against the experimental measurements. A Gaussian

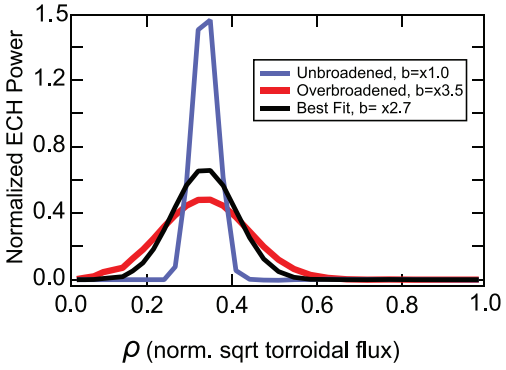

FIG. 2. Power deposition functions for three different degrees of broadening in are shown. The selected diverted L-mode discharge used to evaluate these profiles shows the greatest degree of broadening of any considered for this study will be demonstrated to be b = 2.75.

describes well the initial deposition profile predicted by ray tracing, which can be described by its Gaussian width σ_{TORAY} expressed in ρ or by its FWHM, approximately 2.4× larger—a Gaussian also well describes the time-average scattered profiles seen in simulations of microwave beam scattering.[7] For a deposition profile broadened by a power-conserving Gaussian filter of width σ_F, a broader, yet still Gaussian profile is produced. The ratio of the best fit experimental width to the default TORAY-GA width is taken as the observed broadening factor, b, defined by Eq. (1),

$$b = \frac{\sqrt{\sigma_{TORAY}^2 + \sigma_F^2}}{\sigma_{TORAY}}. \quad (1)$$

For this work, a set of broadening Gaussians with a σ_F ranging from 0.005 to 0.01 were convolved radially with a set power deposition profiles generated for each discharge. This produces a set of candidate profiles with a broadening value from 1 to 4, depending on the inherent deposition width. A comparison of base TORAY-GA deposition for the L-mode 165078 and two broadened profiles is shown in Fig. 2. Use of a range of profiles allows for a set of fits to evaluate the optimal degree of broadening, as will be demonstrated in Sec. IV, showing the black curve to best represent the power deposition.

B. Measuring fluctuations

Measurements of density fluctuations on the millimeter scale are fundamental to quantifying the interaction of radio frequency power and turbulence structure. From the perspective of a fixed measurement frame, turbulence varies rapidly—on a rotation timescale. Edge structures move past the position of the launcher much faster timescale than the plasma responds to heating, altering the deflection of the microwave beam, to which the turbulence appears frozen, about its equilibrium path. Variation in the turbulence observed by an injected beam is much faster than the thermal confinement timescale $\tau_e \approx 100$ ms which governs heating, and current relaxation timescale $\tau_r \approx 1$s which governs current drive.[20] In these experiments, scattering is considered in terms of its time-average effect on the deposition profile, justified given turbulence profiles see no coherent perturbation with the RF power modulation, expected as the cycle of modulation for the applied ECH power is shorter than the turbulence evolution timescales in DIII-D.[28]

Average edge fluctuations in these discharges, tabulated in Sec. IV, are measured by a combination of 2D beam emission spectroscopy (BES)[21] and Doppler backscattering (DBS).[22] BES measures larger scale density fluctuations through beam ion spectroscopy, and is sensitive to a larger scale, low poloidal wavenumber turbulence (corresponding to cm-scale density fluctuations), with $k < 3\,\mathrm{cm}^{-1}$. These measurements are not directly used in this paper, but provide a vital benchmark for turbulence simulations is associated works.[10]

Doppler backscattering measures smaller scale density turbulence with correlation lengths of few millimeters to a centimeter through the scattering of a probe beam, sensitive specificially to interaction with structures with a poloidal wavenumber $1\,\mathrm{cm}^{-1} < k_0\rho_s < 8\,\mathrm{cm}^{-1}$.[22] DBS fluctuation amplitudes were cross-calibrated for this experimental campaign, such that a ×2 increase in signal represents a doubling of fluctuation amplitude, but is not absolutely calibrated to a fluctuation level $\tilde{n}_e/n_e$.

Despite the lack of an absolute value, the DBS fluctuation amplitude is the best available proxy in these discharges for the density of edge structures on the millimeter scale, which have been shown[8] to couple most strongly with 110 GHz beam. Full profiles were not available for all discharges due to issues with some channels. For comparison, cross-calibrated amplitude values were instead generated for each discharge, and the value of the 1D mapped profile averaged about $\rho = 0.95 \pm 0.05$ is taken as a parameter of cross-comparison. It is in this region where scattering-significant fluctuations are expected to be the strongest.[42]

To perform the DBS cross-channel calibrations, a moving metal target mirror is inserted between the launch-receive antenna and the vacuum window. The moving mirror (3–5 cm movement generally) generates a returned DBS signal phasor signal and it is the amplitude of this phasor that is used to normalize the signals with respect to each other. The movement of the mirror is large enough to generate several 2 pi fringes but small enough that the radial range power variation is negligible. Pending simulation work will also show that the mm-scale turbulence measured is consistent with the fractional $\tilde{n}_e/n_e$ perturbation recovered from turbulence modeling.[10]

C. Generating a scaling in fluctuation amplitude

A range of discharge conditions with significantly different edge character can be achieved on DIII-D. Experiments in a series of conditions were used as a means to provide a larger variation in fluctuation amplitude than could readily be achieved in a single discharge. This subsection very briefly describes the edge conditions explored to produce the amplitude scan, represented by the reference discharges in Table I. Parameters of DIII-D reference shot number toroidal field B_t, plasma current I_p, core density $n_{e,0}$, mean neutral beam power P_{NBI},

TABLE I. Reference discharges for the set of conditions used to generate the scaling relation in Sec. IV D. Each reference shape was used for 2–6 discharges with varied aiming, and in some cases modulation rate. The tabulated density is the line averaged value and the total NBI power is held constant. Power is modulated down to 10% of the peak value. For analysis, the calibrated forward power signals are directly analyzed. Also given are the full width half maximum in ρ for the TORAY-GA deposition simulation and the FWHM in ρ of the measured temperature perturbation.

Condition	Ref. Shot	$B_t(T)$	$I_p(MA)$	$n_{e,0}(10^{19}\mathrm{m}^{-3})$	$P_{ECH}(\mathrm{MW})$	W_{TORAY}	W_{FIT}	$\tilde{n}_e DBS$
Limited L-mode	154 532	2.0	1.2	4.2	3	0.055	0.15	12.
Diverted L-mode	165 078	2.0	1	2.9	1.2	0.067	0.15	10.
QH-mode	157 131	1.9	1.1	1.7	1.2	0.045	0.09	8.
ELMy H-mode	165 146	2.0	1.0	3.2	6	0.072	0.12	5.
$-\delta$ L-mode	166 192	2.0	0.9	3.0	0.8	0.046	0.06	3*.

available ECH power P_{ECH}, as well as the full width half maximum in radial coordinate normalized root of toroidal flux, referred to by DIII-D convention as ρ, of the approximately Gaussian simulated and best-fit depositions described in subsequent sections.

L-mode is the basic mode of operation for a tokamak, a simple Ohmic plasma with auxiliary heating at a level below the H-mode transition threshold, producing an extended edge region with a substantial amount of turbulence.[23] A substantial level of fluctuations associated with the extended density gradient at the edge of the machine drives significant turbulent transport.[19] Discharges were considered both before during period of stable sawtoothing, which was treated by blanking the interval around the crash, then fitting and subtracting the background sawtooth perturbation to produce results consistent at the deposition radius.

The formation of a high confinement H-mode is known to be related to $E \times B$ flow suppression of turbulence in the tokamak edge.[24] Consistent with this, the time-integrated edge fluctuation level measured in H-modes between edge localized mode crashes is substantially lower. Averaging over crashes, a narrower, lower amplitude mm-scale turbulence layer is measured.

QH-mode is a modification to H-mode wherein the pedestal is stabilized by a series of oscillations which have been found to lead to increased short-wavelength turbulence.[25] H-mode turbulence data were averaged across the ELM cycle, and in the ELM-perturbed region outside of $\rho = 0.6$, the H-mode data becomes less reliable as the coherent ELM perturbation adds substantial background signal. The coherent effect on RF and the core perturbation profile was observed to be small.[11]

Negative triangularity ($-\delta$) L-mode discharges, a novel concept run on DIII-D, generated the lowest levels of edge fluctuations. These discharges also have relatively good transport for an L-mode plasma, represented by an $H_{98} \approx 1$.[12] Similar discharges on TCV found substantially reduced turbulence was driven by changes in the shape-dependent trapped electron mode drive.[26]

By considering the variation of scattering-relevant fluctuations across discharge conditions, an experimental scaling covering a substantial range in amplitude is produced. In a shape-matched discharge the transition between L- and H-mode is associated with a factor of four drop in fluctuation amplitude measured by Doppler backscattering. Further descriptions, profiles, and equilibrium reconstructions of the matched H- and L-mode discharges can be found in a prior work.[11]

III. USING HEAT PULSES TO RESOLVE MICROWAVE DEPOSITION

A. Perturbation measurements

In a simplified 1D heat conservation representation, the change in electron stored energy driven by power modulation can be calculated as a function of density n_e, and the prompt change in temperature T_e at the switch-on of ECH power P_{ECH}. The no-transport limit (setting the electron heat flux $q_e = 0$) of Eq. (2) is referred to as the instantaneous break in slope, but past measurements of tokamak transport have found this heat flux is always significant on measurable timescales.[3] Transport of heat quickly obscures the deposition profile in this simple limit, producing substantial deviations between high time resolution temperature measurements both between pulses and at turn-on and turn-off,[14]

$$3/2 n_e \frac{\partial T_e(\rho,t)}{\partial t} \approx p_{ECH}(\rho,t) - q_e(\rho,t). \quad (2)$$

The plasma response to modulated electron cyclotron heating is dominated by the 1D temperature perturbation. Coherent variations in electron density, plasma rotation, and density and temperature turbulence on mm and cm scales for modulation frequencies above 20 Hz are an order of magnitude smaller fractionally than the thermal perturbation. Resolving the heat flux as primarily electron temperature response across harmonics of the perturbation frequency can distinguish between beam broadening in the turbulence (which does not vary substantially in time along with the modulation) and heat transport (which evolves in response to applied power).

A 48 channel, absolutely calibrated radiometer provides a 1D T_e profile on the midplane digitized at 500 kHz.[27] Second harmonic X-mode ECE coverage at $B_t = 2$T in DIII-D extends from the high field side to the optically thin scrape-off layer on the low field side outside the last closed flux surface at $\rho = 1$, where ρ is defined as the DIII-D radius normalized to square root of toroidal flux. Individual channels have a radial width of approximately 1 cm or 0.05 in ρ.

The square wave modulation produces a regular heat pulse on ECE. A time-domain perturbation response is observed in steady state for 10 or more pulses, allowing a steady state and perturbed temperature to be calculated (with background subtraction of a low order polynomial), such that $T_e(r,t) = T_e,0(r) + \tilde{T}_e(r,t)$, where $\tilde{T}_e$ represents the time-varying portion perturbation. This perturbation is Fourier analyzed in a set of harmonics of the base modulation frequency f_{MOD}. An example perturbation from this work is compared with the ray-tracing-derived power deposition profile in Fig. 3.

Fourier analysis has been found to produce significantly reduced uncertainties compared with fitting at the on and off times of the power modulation cycle used in earlier work.[14] As shown in Fig. 3 and widely seen in past studies,[3,16] the temperature profiles are wider than

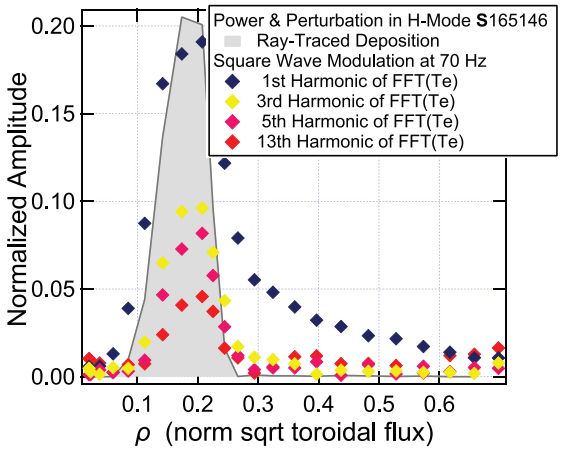

FIG. 3. The Fourier analyzed temperature perturbation generated by a square wave modulation of ECH power with a frequency of 70 Hz. Heating produces a harmonic set of perturbations in electron temperature measured by electron cyclotron emission, with higher harmonics reflecting faster timescale behavior. A subset of the odd harmonics used in fitting are shown, from the base 70 Hz to the highest frequency used up to the 13th harmonic, the highest used.

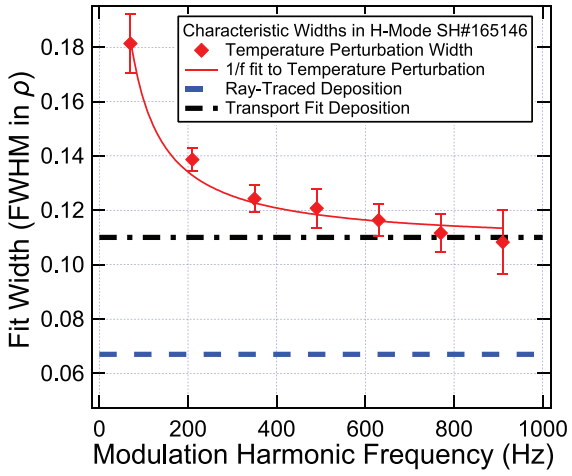

FIG. 4. In an H-mode discharge, a Gaussian fit is made to temperature perturbations produce by ECH and to a base and broadened TORAY-GA deposition profile. A simple fit to the perturbation widths, $FWHM = A/f + FWHM_0$ frequency response is the simple fit to the data, and produces a limit $FWHM_0 = 1.07$, which will subsequently be demonstrated to be comparable to the transport fit $FWHM_0 = 1.07$, both much wider than the TORAY-GA deposition width o $FWHM_0 = 0.67$.

TORAY-GA calculated deposition and expand with decreasing modulation frequency or increasing time. This is in part due to transport effects and as argued in subsequent sections, due to a beam broadening effect driven by scattering from density fluctuations.

A basic fit to the perturbation widths and the ECH profile width calculated by TORAY GA, shown in Fig. 4, suggests that a broadened deposition is consistent with the measured temperatures, as the profile width does not asymptote to the no perturbation limit. The transport fitting value for this discharge better describes this limit and will be calculated in Sec. IV to be $b = 1.7$.

B. Heat flux calculations

Adding heat to the plasma leads to a prompt change in the flow of energy, such that $\partial T_e/\partial t \neq dT_e/dt$. Modulation produces a perturbation to the electron heat flux $\tilde{Q}_e$ which obscures the base deposition profile in the temperature perturbation. The relationship between that flux, stored energy, and the power sources is described by the 1D energy conservation equation, Eq. (3). This formulation includes the heat transport neglected above in Eq. (2),

$$\frac{d}{dt}\left(\frac{3}{2}n_e\tilde{T}_e\right) + \nabla\cdot\tilde{Q}_e = \tilde{p}_{ECH} + \tilde{p}_{OTHER}. \tag{3}$$

This work uses the flux formulation of the heat equation calculated by the integration of the measured temperature perturbation and a trial p_{ECH}. The term $\tilde{p}_{OTHER}$ groups together small terms which contribute more strongly in the slow modulation limit- Ohmic, electron-ion exchange, and other small-amplitude terms are treated as part of the heat flux response in the coupled transport discussed in the subsequent sections.

Using separation of variables in r and t, the time-dependent portions can be Fourier transformed with the kernel $e^{2\pi ift}$ into a harmonic series in modulation frequency, $f = f_{mod} * n$. The perturbed electron heat flux is calculated by integration of Eq. (3) to produce Eq. (4). When treating the transport in cylindrical geometry, the heat flux contains radial factor for geometric expansion which is included in these calculations. A calculation of $\tilde{Q}_e$ is made for each value of the broadening factor to be fit according to the transport model,

$$\tilde{Q}_e(r, f = f_{mod} * n) = \frac{1}{r}\int_0^r \left(\tilde{p}_{ECH}(r', f) - 3i\pi n f_{mod} n_e(r')\tilde{T}_e(r', f_{mod} * n)\right) r' dr. \tag{4}$$

C. Defining transport coefficients

The consistency between an energy conservation-derived 1D heat flux perturbation and a 1D linear transport model which depends on the perturbation is used as the metric to evaluate broadened power deposition.[29] A fit simultaneously across harmonics distinguishes this work from previous efforts, and allows for a clear χ^2 minimization to resolve the deposition broadening. Strictly diffusive models fail to capture the convective heat flux which flows against the gradient in some microwave heated plasmas.[30] Diffusive (denoted by the coefficient D here, although χ is also often used in the literature) and convective (V) components are necessary to capture the effects of microwave heating.[31] Expressing this as an equation for heat flux, q_e gives

$$Q_e(\rho, t) = -Dn_e\nabla T + Vn_eT. \tag{5}$$

The D and V coefficients are not expected to be constant. They can vary both radially and over the power modulation cycle, but depend on a set of tokamak parameters in a complex way which is not known *a priori*.[20] Instead, the dominant temperature perturbation can be used to linearize the plasma response, thereby D and V can be expressed as a set of partial derivatives and dependencies on the temperature perturbation $\tilde{T}_e$ and its gradient.[32] Sorting terms by their dependence on the temperature perturbation produces the following equation:

$$\tilde{Q}_e/n_e = -\nabla\tilde{T}_e\left(D + \nabla T_e\frac{\partial D}{\partial\nabla T_e}\right) + \tilde{T}_e\left(V + T_e\frac{\partial V}{\partial T_e} - \nabla T_e\frac{\partial D}{\partial T_e}\right) + \nabla\tilde{n}_e\left(T_e\frac{\partial V}{\partial\nabla n_e} - \nabla T_e\frac{\partial D}{\partial\nabla n_e}\right) + \tilde{n}_e\left(T_e\left(\frac{V}{n_e} + \frac{\partial V}{\partial n_e}\right)\right). \tag{6}$$

The resulting linearized equation is still too complicated to be fit readily, but terms can be grouped based on the order of their dependency on the perturbation $\tilde{T}_e$ and reduced to simple locally constant or radial polynomial coefficients which are independent of frequency. A term proportional to $\tilde{T}_e$, to $\nabla\tilde{T}_e$, and one which depends on neither can capture the full set of dependencies the fitting of the subsequent sections. These terms, expressed as V_M, D_M, ξ can be understood as the modulated convective, diffusive, and coupled transport terms, respectively. This 3-term transport model has been employed for over a decade on DIII-D with good consistency generally found with existing transport codes.[20,34]

The modulated diffusion term can be assembled from all terms proportional to $\nabla\tilde{T}_e$. This diffusivity is comparable to the TEM-driven critical gradient response seen by Hillesheim[33] and by deBoo *et al*[34] in transport studies on DIII-D - driving a heat flux response

with diffusion coefficients greater than 15 times the gyro-Bohm level in a prompt response to the temperature perturbation. This perturbation-dependent response enters in the second term of Eq. (7),

$$D_M = D + \nabla T_e \frac{\partial D}{\partial \nabla T_e}. \tag{7}$$

Similarly, a modulated convection can be assembled from all terms containing $\tilde{T}_e$ as Eq. (8), which can capture both positive and negative transport coefficients like those seen in the studies of Mantica *et al.*,[30]

$$V_M = V + T_e \frac{\partial V}{\partial T_e} - \nabla T_e \frac{\partial D}{\partial T_e}. \tag{8}$$

Coupled transport, written as the complex, frequency-dependent coefficient ξ, contains terms driven by the modulated density and its gradient, and functionally captures other small corrections coherent with the power modulation.[20] These are grouped together as ξ, Eq. (9) for the fit as they are functionally independent of the temperature perturbation,

$$\xi/n_e = \nabla\tilde{n}_e\left(T_e\frac{\partial V}{\partial \nabla n_e} - \nabla T_e \frac{\partial D}{\nabla n_e}\right) + \tilde{n}_e\left(T_e\left(\frac{V}{n_e} + \frac{\partial V}{\partial n_e}\right)\right) + \xi_{OTHER}. \tag{9}$$

The ξ term has an unknown frequency dependence following from dependencies on $\nabla\tilde{n}_e$ and $\tilde{n}_e$, and potentially other effects such as flux surface modulation or fast transport, expressed as ξ_{OTHER}. The frequency dependence and relative phase of the density evolution to the power modulation is difficult to determine apriori. As used in past ballistic heat pulse work by Fredrickson,[35] an exponential decay with a free phase can capture the dominant time response of the coupled transport.

This term could also in principle capture the effects of fast electron transport modification to diffusion, or terms w. The exponential decay of the form $f(t) = A * \exp(-|c|(t - t_0))$ has a Fourier transform $F(f) = 2A/(c + i2\pi f)$. Representing the complex number as a phase term θ_ξ, and the amplitude as $\xi_0 = A\sqrt{c^2 + (2\pi f)^2}$ allows simplification to the fitting form of ξ which can reflect a $1/f$ or $1/f^2$ frequency dependence depending on the relative magnitude of the characteristic response frequency, c, and the modulation harmonic frequency, f,

$$\xi(r,f) = \xi_0(r) \times e^{i\theta_\xi} \times \frac{4\pi c}{4\pi f_{mod}^2 + c^2}. \tag{10}$$

Here ξ_0 is a constant with units of heat flux seconds, θ_ξ is a phase relative to the ECH power modulation, and c is a constant with units of frequency. Writing a fit term with this freedom allows a ballistic population without enforcing it––a scaling with bulk density occurs for small values of c producing a 1/f response, whereas fast transport will generally scale-like frequency squared. Estimates for ITER parameters suggest that the level of fast electron transport predicted ($D_{rr} \approx 0.15\,\mathrm{m^2 s^{-1}}$) will not lead to a substantial broadening of the ECCD profile.[36]

DIII-D ECCD studies which did not treat fluctuation broadening capped the levels of diffusive transport for fast electrons at a modest $D_{rr} = 0.4\,\mathrm{m^2\,s^{-1}}$,[37] while admitting that the actual level may be somewhat lower. While transport at this level can drive profile broadening, a value of $D_{rr} = 1.0\,\mathrm{m^2\,s^{-1}}$ is considered the minimum level for deleterious broadening[36] comparable to the magnitude of broadening observed in this work. The broadening for L-mode is consistent with within uncertainties for both core and edge deposition in DIII-D,[11] whereas the work of Harvey *et al*[38] predicts two orders of magnitude difference between edge and core current diffusion times. If diffusion of hot particles confounded broadening estimates, *b* factors for core and edge deposition would differ, which is not seen in these experiments.

IV. TRANSPORT FITTING RECOVERS BROADENED DEPOSITION

A. Methodology

In this section, we apply self-consistency of power conservation and linear transport heat fluxes to evaluate broadening in a set of DIII-D discharges. Writing the heat flux in this simplified form produces a three-term Eq. (12) which will be evaluated against the power conservation derived heat flux [Eq. (4)] to produce Eq. (11). This equation is fit across the first 4–6 harmonics of the Fourier basis of the modulated ECH power across the reference discharges of Table I. Harmonics are included in the fit when a $>2\sigma$ temperature perturbation is seen, and discarded otherwise, producing 3–6 fittable harmonics for the cases considered:

$$\begin{aligned}\tilde{Q}_e(r,t)/n_e(r,t) &= -D_M\nabla\tilde{T}_e + V_M\tilde{T}_e + \xi \\ &= \frac{1}{rn_e}\int_0^r \left(\tilde{p}_{ECH}(r', f_{mod} * n) - 3i\pi N F_{mod} n_e(r')\tilde{T}_e(r', f_{mod} * n)\right) r'dr'.\end{aligned} \tag{11}$$

Based on a set of broadened deposition profiles, the agreement between the transport model is evaluated. The best fit value is the one that produces consistency between energy conservation and linear transport expressions of the heat flux. In the formulation of the power balance heat fluxes, a cylindrical geometry is used. A local fit equation consists of five terms at least (D_M, V_M, amplitude, phase, and characteristic time of ξ), with good agreement between locally constant and radially varying polynomial forms of the coefficients in this and past studies.[11] This fit is made for a range of values of broadening factors, b, with the goodness of fit parameter, χ^2 used to compare values of b.

An example of the best fit case for an H-mode case is shown in Fig. 5. Local constant coefficients fit inside or outside of the deposition region generate reduced χ^2 consistent with a quality minimization. When considering radial variation, 6 term radial polynomial coefficients are sufficient to produce an over-fit, with $P(\chi^2 > \chi^2_{fit} = 0.3 - 0.05)$ but their values agree well with locally constant coefficients. Fits are performed in the 'x+iy' form of the complex equation—with the real and complex value at each ECE channel in the deposition region and each odd harmonic of the modulation frequency,

$$\begin{aligned}D_M\nabla\tilde{T}_e(r,f) + V_M\tilde{T}_e(r,f) + \xi(r,f) \\ = \frac{1}{rn_e}\int_{r'=0}^{r}(\tilde{p}_{ECH}(r',f) - 3i\pi f n_e(r')\tilde{T}_e(r',f))r'dr.\end{aligned} \tag{12}$$

The fit values for χ^2 shows a clear minimum at a differing degree of broadening across the range of discharge conditions. Figure 6 shows an example of the broadening factors explored for an L-mode shot in which power was deposited in matched conditions in either the core

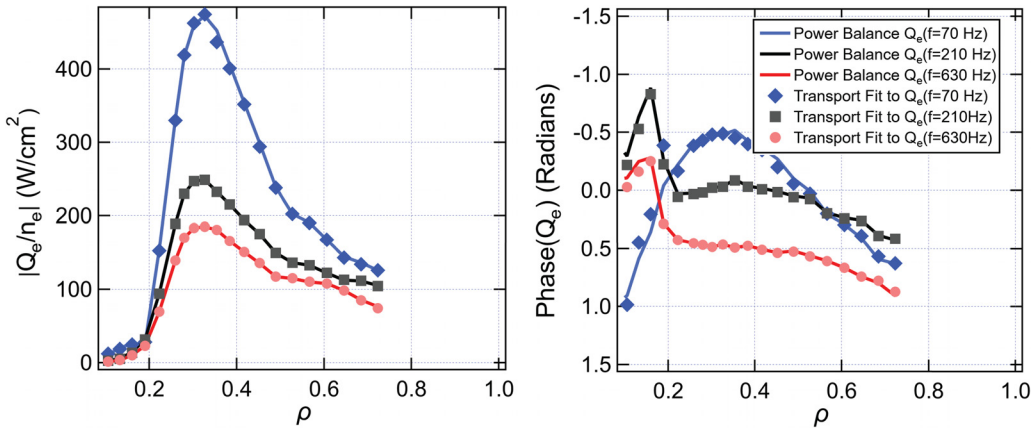

FIG. 5. Calculated and fit values of electron heat flux amplitude and phase for a 5 term radial polynomial fit to the three parameters, with a radially constant phase and characteristic time for ξ. The fit is made to 22 radial locations and 9 frequency harmonics, which have been downselected in plotting for legibility. Good agreement is achieved between the transport fit values (markers), and the power balance values (lines). Above the ninth harmonic, uncertainties are comparable to the calculated fluxes and these values are not fit.

or the edge. The perturbation profile widths (defined as the FWHM of the perturbation profile, $\frac{3}{2} n_e dT_e/dt$) for the two cases differ substantially, as does the transport in the deposition region, but a consistent broadening is found, $b \approx 2.75$. All discharges studied have a similar minimization, although broadening factors fit vary from $\times 1.4 - \times 2.9$. Broadening to a degree that minimizes χ^2 is also found to produce consistently positive modulated diffusion coefficients.

B. Comparison of coefficients with the differential heat transport formulation

Validation of the heat flux fitting method has been performed against a set of discharges analyzed in a previous DIII-D study.[34] A

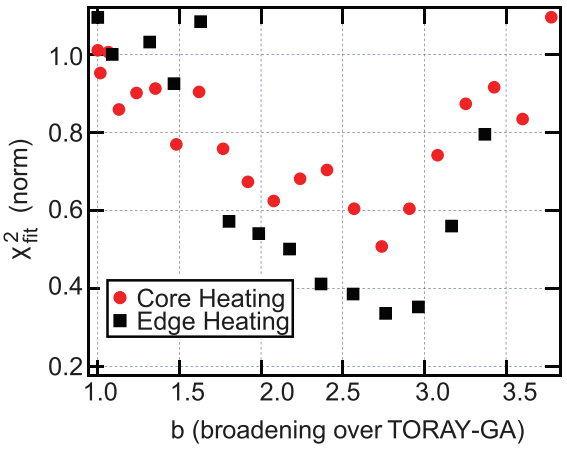

FIG. 6. χ^2 minimization is used as a means of comparing different degrees of broadening, b, the x-axis, in a matched discharge with two different deposition locations. When power is applied in L-mode discharge near the core ($\rho = 0.25$) or at the same power near the edge ($\rho = 0.6$) in same plasma, inherent widths of deposition differ sharply due to changes in plasma parameters and geometry, and transport coefficients vary between the two regions. However, fitting finds the same broadening factor, x2.75 broader deposition in ρ, produces the best agreement in both cases.

scan of gyrotron aiming was used to alter the temperature gradient at the plasma edge. Power was incrementally moved from edge to mid-radius to steepen the gradient, producing the "critical gradient" behavior, where transport coefficients are found to be a function of temperature gradient above a certain value of scale length $L_{T_e} = (\partial T_e/\partial r)/T_e$. Results from this study, based on the differential form of the heat equation, can be used as a benchmark for the integral heat flux method presented here.

As with the integral method of thermal transport used in this work, the second order ODE method uses a three term fit to a modulated diffusion D_{HP}, convection V_{HP}, and an additional damping term proportional to the temperature perturbation $\tilde{T}_e$ and written as $1/\tau$. In this form, a second derivative of $\tilde{T}_e$ appears instead of an integral, as fitting a diffusive transport equation requires consideration of three orders in differentiation,

$$-D_{HP}\nabla^2\tilde{T}_e + V_{HP}\nabla\tilde{T}_e + \tilde{T}_e\left(3\pi fi + \frac{1}{\tau}\right) = \tilde{p}_{ECH}/n_e. \quad (13)$$

For a Monte Carlo integral as performed in the heat flux method, error bars are directly calculated from the standard deviation of the random draw. Minimizing intrinsic uncertainty in the fit equation improves the method's sensitivity to changes in power deposition. The differential form uses an analytic solution fit to the measured perturbation. However, the integral and differential form of the diffusion coefficients is directly comparable.

With a locally constant fit, $\int D_{HP}\nabla^2\tilde{T}_e dx$ is directly comparable to $D_M\nabla\tilde{T}_e$. In a set of discharges, a constant coefficient was fit from $\rho = 0.25$ to $\rho = 0.6$ was made with both methods. The results for the diffusion coefficient are given in Fig. 7. It is found that the integral method reproduces the same critical gradient value and response found by the differential method, despite differences in fit methodology.

C. Fit transport coefficients

Transport coefficients in tokamaks such as DIII-D[5] and TFTR[35] were found to vary by an order of magnitude over the plasma radius. While locally constant coefficients like those in the last Sec. are useful,

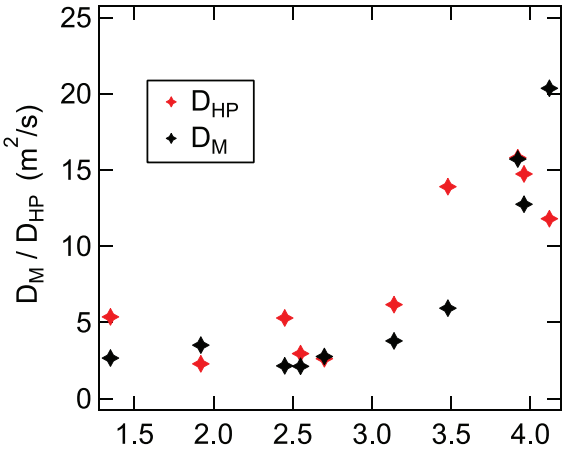

FIG. 7. Heat flux transport fitting can reproduce the critical gradient results from previous DIII-D heat transport studies.[34] The modulated diffusivity measured at $\rho = 0.6$ increases sharply above the Gyro-Bohm level of 4 m^2/s as the electron temperature scale length, L_{T_e} approaches a critical value, here found to be $\approx 2.5\,m^{-1}$. The differential and flux integral method fits of diffusion coefficient are evaluated in a slab geometry from $\rho = 0.45$ to $\rho = 0.75$. The integral method produces reduced scatter vs the previous method involving a second derivative of the ECE data.

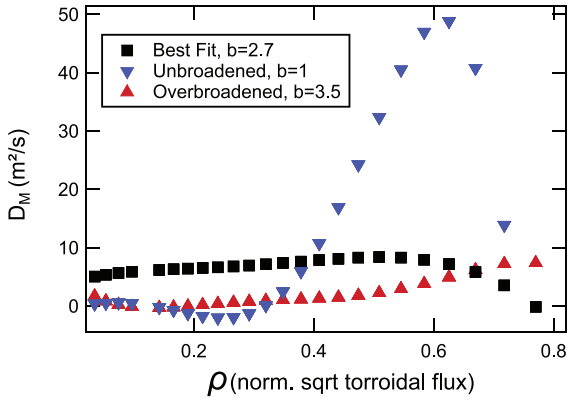

FIG. 8. In this L-mode case, D_M is fit with polynomial as a function of ρ. D_M is strongly sensitive to the chosen broadening, as the gradient of the perturbation $\nabla \tilde{T}_e$ flips phase across the deposition region. Radially increasing, consistently positive values of D_M for a significantly broadened L-mode coincide with minimization of χ^2.

the simultaneously fitting of the full dataset requires the ability to treat radial variation. This can be done by fitting a set of orthogonal polynomials, with coefficients found applying both methods found to be consistent with local polynomials.[11]

An example of a radial fit of D_M in the diverted L-mode discharge for various choices of b is shown in Fig. 8. Polynomial fit results for the diffusion coefficients enforce consistency in heat flux in and outside of the deposition region but depend most strongly on the deposition region where relative amplitudes of the perturbation are large.

When a b-factor larger than the optimal is applied, diffusion again goes negative, but in this case outside the deposition region at $\rho = 0.2$—over-broadening has moved too much power into the core, and a negative diffusion in this region is required to account for a physically broadened deposition. It must be noted that ECE temperature measurements generally become optically thin outside of $\rho = 0.9$, providing an outer bound on the validity of the analysis.

An example of all three coefficients fit with fourth-order polynomial radial variation is shown in Fig. 9 for a QH-mode case. While the modulated convection and coupled transport do not readily compare to their non-modulated equivalents, they are provided for the reader. These coefficients are for the best fit case, but the use of only one modulated gyrotron limits fitting to the first four harmonics of the base perturbation frequency $f_{mod} = 28$ Hz.

Negative triangularity shows the lowest degree of fluctuation broadening along with a reduced level of global transport, as expressed by an $H_{(95)}$ which can exceed 1 in L-mode.[12] This is reflected in its reduced D_M and V_M compared with the standard L-mode case as shown in Fig. 10. Also shown is the coupled transport term for negative triangular, which constitutes about 30% of the modulated heat flux.

Additional fit results using locally constant coefficients are presented in Sec. IV B. Basic matched L- and H-mode cases can be found in previous work.[11]

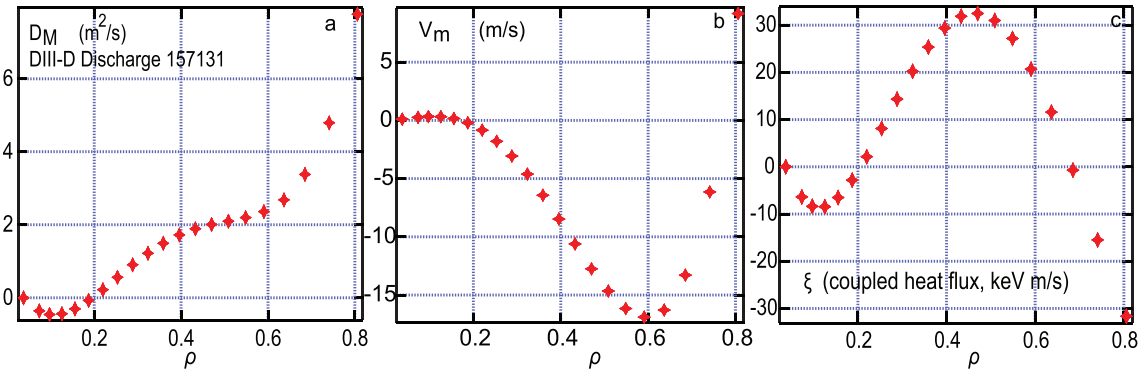

FIG. 9. This QH-mode modulated diffusion (a) and convection coefficients (b) show a substantially reduced levels of heat pulse transport vs the L-mode in Fig. 8, consistent with the expectation of improved confinement in H-mode. Coupled transport (c) constitutes less than 20% of the total flux. The best fit trace is shown in this example.

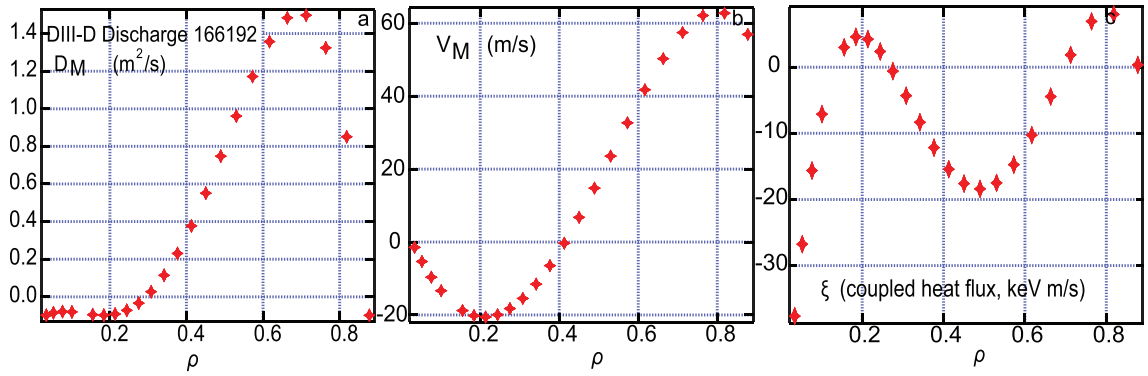

FIG. 10. Modulated diffusion (a), convection (b), as well as the frequency independent amplitude of the coupled transport coefficient(c) are plotted for the negative triangularity case. Negative triangularity shows H-mode level confinement ($H_{98} > 1.0$) in L-mode.[12] The diffusive coefficient has a negative value in the core, but this is far from the target deposition region of $\rho = 0.5$, suggesting this excursion is independent of the chosen broadening.

D. Identifying a scaling with fluctuation level

A range of deposition powers and locations within five edge conditions have been examined to produce a beam broadening scaling with a cross-calibrated fluctuation amplitude in the edge ($\rho \approx 0.95$). Figure 11 shows broadening factors derived from these fits assembled by discharge condition. Uncertainties in the experimental broadening value are derived from the increment in χ^2, and are limited to the resolution of the grid used to evaluate the χ^2 minimization. Fit ranges are selected to avoid any magnetic islands as well as the ELM-perturbed edge of H-mode plasmas, which can extend in as far as $\rho = 0.6$.[39] A nominal ± 1 amplitude uncertainty in the DBS data are derived from the variation over time in the simulated turbulence found in the simulation of these discharges.[40]

The experimental scaling of broadening with DBS-derived fluctuations shown in Fig. 11 is roughly linear, but a quadratic scaling fits the data nearly as well. A linear scaling was predicted by J. Decker with the LUKE-C3PO code.[7] Work performed using full-wave codes suggests a quadratic trend.[8] When considering the combination of fluctuation layer thickness and local fluctuation amplitude $A = \tilde{n}_e/n_e$, the discharges are still approximately consistent with quadratic amplitude dependence for the scattering parameter as found by past effort[8] within the uncertainties.

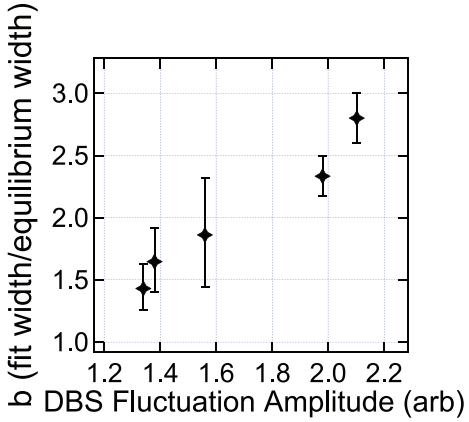

FIG. 11. A collection of discharges in five conditions have both fluctuation data and modulation needed to form a scaling. Broadening of the narrow RF beam used in deposition calculated in TORAY-GA will lead to a corresponding increase in deposition width. The horizontal axis is the normalized density fluctuation amplitude from the Doppler backscattering system at $\rho = 0.95$. The broadening factor is defined as the ratio of the best fit deposition profile FWHM to the TORAY-GA value.

In an accompanying paper in preparation now,[40] a 3D full-wave cold plasma finite difference time domain code EMIT-3D[41] has been used to simulate the extent to which scattering broadens a microwave beam in DIII-D, and it discusses the effects of turbulence layer thickness in greater depth. A full-wave treatment is necessary when the inhomogeneity scale length is comparable to the wavelength,[8] explaining why these profiles are wider than those found by past simulation efforts.[4]

V. CONCLUSIONS

In this work, a linear transport model was used to fit the electron heat flux generated by electron cyclotron heating. The best fit to a transport model accounting for RF beam broadening is assessed with a three term model that includes diffusion, convection, and coupled transport effects, finding a broadened deposition that scales linearly with density fluctuation amplitude across a range of discharge conditions. The simulation paper accompanying this work finds a consistent degree of broadening in 3 DIII-D cases where a "full wave" propagation analysis solving Maxwell's equations has been performed.[40] Deposition width in normalized minor radius ρ was found to be $\times 1.4$–2.75 wider than predicted by ray tracing through a no-fluctuation equilibrium, increasing linearly with edge turbulence amplitude in both cases.

The observed degree of broadening leads to an increase in power requirements for mode control met readily on existing devices, but which could increase power requirements and motivate different EC launch strategies on future devices. Future work predicting this effect and other non-equilibrium effects such as current condensation[13] appear necessary to make well-founded predictions for next-step devices. While scattering broadens the beam in the transverse direction, condensation could reduce the radial extent of the absorption layer, with the magnitude of the competing effects depending on the geometry of the beam.

Direct measurement of the broadened RF beam in the DIII-D edge may soon be possible.[43] Results from these experiments highlight the significance of fluctuation scattering to current drive localization and are being used to validate a set of simulation tools to model this effect in current and future devices.

ACKNOWLEDGMENTS

This material is based upon work supported by the U.S. Department of Energy, Office of Science, Office of Fusion Energy Sciences, using the DIII-D National Fusion Facility, a DOE Office of Science user facility, under Award Nos. DE-FC02–04ER54698 and DE-FG03–97ER54415.

This report was prepared as an account of work sponsored by an agency of the United States Government. Neither the United States Government nor any agency thereof, nor any of their employees, makes any warranty, express or implied, or assumes any legal liability or responsibility for the accuracy, completeness, or usefulness of any information, apparatus, product, or process disclosed, or represents that its use would not infringe privately owned rights. Reference herein to any specific commercial product, process, or service by trade name, trademark, manufacturer, or otherwise does not necessarily constitute or imply its endorsement, recommendation, or favoring by the United States Government or any agency thereof. The views and opinions of authors expressed herein do not necessarily state or reflect those of the United States Government or any agency thereof.

DATA AVAILABILITY

The data that support the findings of this study are available from the corresponding author upon reasonable request.

REFERENCES

[1]G. Gantenbein, H. Zohm, G. Giruzzi, S. Günter, F. Leuterer, M. Maraschek, J. Meskat, and Q. Yu, Phys. Rev. Lett **85**, 1242 (2002).
[2]U. Stroth, L. Giannone, and H.-J. Hartfuss, Plasma Phys. Controlled Fusion **38**, 611 (1996).
[3]M. Zerbini, M. Austin, S. Bernabei, G. Giruzzi, M. Murakami, J. Lohr, T. C. Luce, C. C. Petty, D. Ponce, and R. Prater, Plasma Phys. Controlled Fusion **41**, 931 (1999).
[4]R. Prater, D. Farina, Y. Gribov, R. W. Harvey, A. K. Ram, Y.-R. Lin-Liu, E. Poli, A. P. Smirnov, F. Volpe, E. Westerhof, and A. Zvonkov, Nucl. Fusion **48**, 035006 (2008).
[5]K. W. Gentle and M. E. Austin, Phys. Plasmas **13**, 012311 (2006).
[6]M. van Berkel, T. Kobayashi, G. Vandersteen, H. J. Zwart, H. Igami, S. Kubo, N. Tamura, H. Tsuchiya, and M. R. de Baar, Nucl. Fusion **58**(9), 096036 (2018).
[7]J. Decker, Y. Peysson, and S. Coda, EPJ Web Conf. **32**, 01016 (2012).
[8]A. Köhn, E. Holzhauer, J. Leddy, M. B. Thomas, and V. RGL, Plasma Phys. Controlled Fusion **60**, 075006 (2018).
[9]O. Chellaï, S. Alberti, M. Baquero-Ruiz, I. Furno, T. Goodman, F. Manke, G. Plyushchev, L. Guidi, A. Köhn, O. Maj, E. Poli, K. Hizanidis, L. Figini, and D. Ricci, Phys. Rev. Lett. **120**, 105001 (2018).
[10]M. W. Brookman, M. B. Thomas, M. E. Austin, K. Barada, K. W. Gentle, L. Holland, R. J. La Haye, J. B. Leddy, C. C. Petty, T. L. Rhodes, Z. Yan, A. Köhn-Seemann, and R. G. L. Vann, Phys. Rev. Lett. (submitted) (2020).
[11]M. W. Brookman, M. E. Austin, K. W. Gentle, C. C. Petty, D. E. Ernst, Y. Peysson, J. Decker, and K. Barada, EPJ Web Conf. **147**, 03001 (2017).
[12]M. E. Austin, A. Marinoni, M. L. Walker, M. W. Brookman, J. S. deGrassie, A. W. Hyatt, G. R. McKee, C. C. Petty, T. L. Rhodes, S. P. Smith, C. Sung, K. E. Thome, and A. D. Turnbull, Phys. Rev. Lett. **122**, 115001 (2019).
[13]A. H. Reiman and N. J. Fisch, Phys. Rev. Lett **121**, 225001 (2018).
[14]M. W. Brookman, M. E. Austin, and C. C. Petty, AIP Conf. Proc. **1689**, 090005 (2015).
[15]L. Vahala, Phys. Fluids B. **4**, 619 (1992).
[16]K. K. Kirov, F. Leuterer, G. V. Pereverzev, F. Ryter, and W. Suttrop, Plasma Phys. Controlled Fusion **44**, 2583 (2002).
[17]E. Kolemen, A. S. Welander, R. J. La Haye, N. W. Eidietis, D. A. Humphreys, J. Lohr, V. Noraky, B. G. Penaflor, R. Prater, and F. Turco, Nucl. Fusion **54**, 073020 (2014).
[18]E. Poli, C. Angioni, F. J. Casson, D. Farina, L. Figini, T. P. Goodman, O. Maj, O. Sauter, H. Weber, H. Zohm, G. Saibene, and M. A. Henderson, Nucl. Fusion **55**(1), 013023 (2015).
[19]B. D. Dudson and J. Leddy, Plasma Phys. Controlled Fusion **59**, 054010 (2017).
[20]T. C. Luce, J. C. DeBoo, N. Howard, C. Liu, and C. C. Petty, in ECA (2005), Vol. **29C**, p. P-5.038.
[21]G. R. McKee, R. J. Fonck, D. K. Gupta, D. J. Schlossberg, M. W. Shafer, R. L. Boivin, and W. Solomon, Plasma Fusion Res. **2**, S1025 (2007).
[22]W. A. Peebles, T. L. Rhodes, J. C. Hillesheim, L. Zeng, and C. Wannberg, Rev. Sci. Instrum. **81**, 10D902 (2010).
[23]J. Wesson, *Tokamaks* (Oxford Science Publications, 2011).
[24]T. L. Rhodes, J.-N. Leboeuf, R. D. Sydora, R. J. Groebner, E. J. Doyle, G. R. McKee, W. A. Peebles, C. L. Rettig, L. Zeng, and G. Wang, Phys. Plasmas **9**, 2141 (2002).
[25]J. C. Rost, M. Porkolab, J. Dorris, and K. H. Burrell, Phys. Plasmas **21**, 062306 (2014).
[26]A. Marinoni, S. Brunner, Y. Camenen, S. Coda, J. P. Graves, X. Lapillonne, A. Pochelon, O. Sauter, and L. Villard, Plasma Phys. Controlled Fusion **51**, 055016 (2009).
[27]M. E. Austin and J. Lohr, Rev. Sci. Instrum. **74**, 1457 (2003).
[28]D. R. Ernst, K. H. Burrell, W. Guttenfelder, T. L. Rhodes, L. Schmitz, A. M. Dimits, E. J. Doyle, B. A. Grierson, M. Greenwald, C. Holland, G. R. McKee, R. Perkins, C. C. Petty, J. C. Rost, D. Truong, G. Wang, and L. Zeng, in Proceedings of the 25th International Atomic Energy Agency Fusion Energy Conference (2014).
[29]R. E. Stockdale, K. H. Burell, and W. Tang, Bull. Am. Phys. Soc. **31**, 1535 (1986).
[30]P. Mantica, A. Thyagaraja, J. Weiland, G. M. D. Hogeweij, and P. J. Knight, Phys. Rev. Lett. **95**, 185002 (2005).
[31]F. Ryter, T. Pütterich, M. Reich, A. Scarabosio, E. Wolfrum, R. Fischer, M. Gemisic Adamov, N. Hicks, B. Kurzan, C. Maggi, R. Neu, V. Rohde, and G. Tardini, Nucl. Fusion **49**, 062003 (2009).
[32]K. W. Gentle, Phys. Fluids **31**, 1105 (1988).
[33]J. C. Hillesheim, J. C. DeBoo, W. A. Peebles, T. A. Carter, G. Wang, T. L. Rhodes, L. Schmitz, G. R. McKee, Z. Yan, G. M. Staebler, K. H. Burrell, E. J. Doyle, C. Holland, C. C. Petty, S. P. Smith, A. E. White, and L. Zeng, Phys. Rev. Lett. **110**, 045003 (2013).
[34]J. C. DeBoo, C. C. Petty, A. E. White, K. H. Burrell, E. J. Doyle, J. C. Hillesheim, C. Holland, G. R. McKee, T. L. Rhodes, L. Schmitz, S. P. Smith, G. Wang, and L. Zeng, Phys. Plasmas **19**, 082518 (2012).
[35]E. D. Fredrickson, A. C. Janos, K. M. McGuire, S. D. Scott, G. Taylor, and Z. Chang, Nucl. Fusion **33**, 1759 (1993).
[36]F. J. Casson, C. Angioni, E. A. Belli, R. Bilato, P. Mantica, T. Odstrcil, T. Puetterich, M. Valisa, L. Garzotti, C. Giroud, J. Hobirk, C. F. Maggi, J. Mlynar, and M. L. Reinke, Nucl. Fusion **55**, 012002 (2015).
[37]C. C. Petty, M. E. Austin, J. Lohr, T. C. Luce, M. A. Makowski, R. Prater, R. W. Harvey, and A. P. Smirnov, Fusion Sci. Tech **57**(1), 10 (2010).
[38]R. W. Harvey, O. Sauter, R. Prater, and P. Nikkola, Phys. Rev. Lett. **88**, 205001 (2002).
[39]A. W. Leonard, Phys. Plasmas **21**, 090501 (2014).
[40]M. B. Thomas, M. W. Brookman, M. E. Austin, A. Köhn, R. J. La Haye, J. B. Leddy, R. G. L. Vann, and Z. Yan, Nucl. Fusion (submitted); preprint arXiv:1710.03028.
[41]T. R. N. Williams, A. Köhn, M. R. O'Brien, and R. G. L. Vann, Plasma Phys. Controlled Fusion **56**, 075010 (2014).
[42]A. Snicker, E. Poli, O. Maj, L. Guidi, A. Köhn, H. Weber, G. Conway, M. Henderson, and G. Saibene, Nucl. Fusion **58**, 016002 (2018).
[43]E. H. Martin, C. Lau, M. W. Brookman, and J. Lohr, Rev. Sci. Instrum. **89**(10), 10D117 (2018).